

# Fluid driven fingering instability of a confined elastic meniscus

JOHN S BIGGINS<sup>1</sup>, Z WEI<sup>2</sup>, L MAHADEVAN<sup>2,3</sup>

<sup>1</sup> *Cavendish Laboratory, JJ Thomson Ave, University of Cambridge, Cambridge, CB3 0HE, United Kingdom*

<sup>2</sup> *School of Engineering and Applied Sciences, Harvard University, Cambridge, MA 02138, USA*

<sup>3</sup> *Department of Physics, Harvard University, Cambridge, MA 02138, USA*

*lm@seas.harvard.edu*

PACS 46.32.+x – Mechanical instability

PACS 46.25.-y – Elasticity in continuum mechanics of solids

PACS 46.55.+d – Adhesion and mechanical contacts (structural mechanics)

**Abstract** – When a fluid is pumped into a cavity in a confined elastic layer, at a critical pressure, destabilizing fingers of fluid invade the elastic solid along its meniscus [1]. These fingers occur without fracture or loss of adhesion and are reversible, disappearing when the pressure is decreased. We develop an asymptotic theory of pressurized highly elastic layers trapped between rigid bodies in both rectilinear and circular geometries, with predictions for the critical fluid pressure for fingering, and the finger wavelength. Our results are in good agreement with recent experimental observations of this elastic interfacial instability in a radial geometry. Our theory also shows that, perhaps surprisingly, this lateral pressure driven instability is analogous to a transverse displacement driven instability of the elastic layer. We verify these predictions by using nonlinear finite-element simulations on the two systems which show that in both cases the fingering transition is first-order (sudden) and hence has a region of bistability.

In continuum mechanics, fingering instabilities are usually associated with interfacial flows in porous media, or its analog, flow in a Hele-Shaw cell. Indeed, the prototypical Saffman-Taylor interfacial instability is associated with a less viscous fluid pushed into a more viscous liquid in a confined geometry, leading to the interface between the two developing finger like protrusions [2, 3], with a wavelength set by a balance between viscous stresses and surface tension [2]. The fingers show various morphologies as a function of the fluid properties, e.g. in the limit of high viscosity contrast and minimal surface tension, or when the fluid is viscoelastic, shear-thinning or viscoplastic, one sees a range of finger, fracture and fractal like patterns [4–18]. Crucially, we note that these instabilities are all manifestations of fluid-like irreversible rate-dependent deformations.

Recently the solid/elastic analog of the Saffman-Taylor experiment has been explored by slowly pumping air into a cavity in a strongly adherent highly-elastic layer in a Hele-Shaw cell [1]. The cavity first dilates laterally and at a critical pressure, fingers of air invaded the elastic layer without fracture or loss of adhesion, as shown in Fig. 1. When the pressure was released the cavity completely recovered its original shape, the hallmark of a purely elas-

tic quasi-static transition. Two other fingering transitions have been reported in soft solid layers sitting betwixt rigid bodies which are then pulled apart. In one peeling causes adhesion between the layer and body to fail, and finger-like undulations appear along the resulting contact line [18–20]. In the other, adhesion is maintained and finger-like invaginations appear at the layer’s perimeter [21, 22]. Here we provide a theory for the fluid-driven reversible elastic instability of a confined meniscus, and unify fingering in strongly adherent elastic layers produced by either pressure driven fluid invasion or transverse displacement. Though familiar from fluids, this unification is unexpected in elasticity where force and displacement loadings typically give different behaviors. While the fingering of polymeric fluids in the limit of high Deborah numbers (when the polymer cannot relax) [6, 16–18] might seem to be similar to the rate-independent elastic deformations treated here, they are not since the former leads to irreversible deformations while the latter is completely reversible.

We begin with scaling estimates for fluid-driven elastic fingering in a thin incompressible neo-Hookean annular layer (Fig. 1a-b) adhered to rigid plates at  $z = \pm a/2$  and with in-plane extent  $r_1 < r < r_2$  ( $r_1 \gg a$ ) and shear modulus  $\mu$ . Since adhesion is maintained, an in-plane

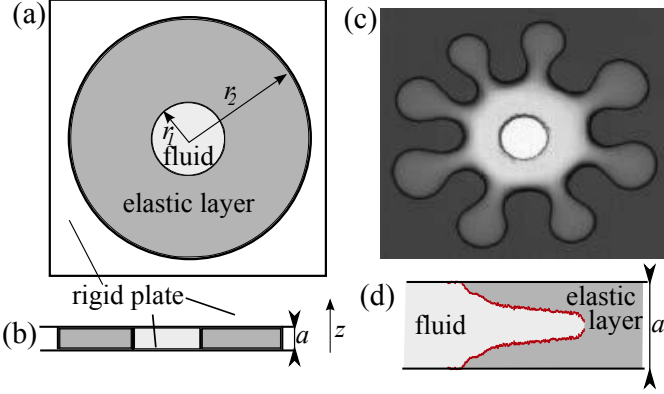


Fig. 1: (a) Top-view of the experiment used to study the elastic analog of Saffman-Taylor fingering [1]: two rigid plates confine a thin elastic layer with a central cavity containing fluid whose volume is increased by injecting fluid from above. (b) Cross-section showing the thickness of the layer. (c) Experimentally obtained finger pattern [1]. The central hole indicates the original cavity size, while the varying gray scale is a consequence of the elastic meniscus deforming without loss of adhesion to the plates. (d) Cross-section of a finger [1] showing maintained adhesion even when the finger amplitude is large, well past the onset of the instability.

displacement  $u$ , applied mid-way between the plates, will generate strains  $\gamma \sim u/a$  localized in-plane by an elastic screening length of  $\mathcal{O}(a)$ , which we expect to be the finger wavelength scale. A fluid (pressure  $P_f$ ) pumped into the cavity will induce such a displacement radially on the inner circumference, increasing its volume by  $\delta V_f \sim 2\pi r_1 u a$ . Since the layer is incompressible, this displacement decays radially as  $u(r) \sim u r_1 / r$ . Equating the layer elastic energy,  $E \sim a \int_{r_1}^{r_2} \frac{1}{2} \mu \gamma^2 2\pi r dr \sim \mu u^2 r_1^2 \log(r_2/r_1)/a$ , and the work done by the fluid,  $P_f \delta V_f$ , yields  $u \sim (P_f/\mu) a^2 / (r_1 \log(r_2/r_1))$ . Since fingering occurs when the strain is finite, i.e.  $\gamma \sim u/a \gtrsim 1$ , this yields a critical threshold pressure for the instability  $P_f \sim \mu (r_1/a) \log(r_2/r_1)$ .

To verify and improve these estimates, we build a minimal 2-d theory, taking advantage of the scale separation induced by confinement. Consider a point with position  $\mathbf{R} = \mathbf{r} + z\hat{\mathbf{z}}$ , and displacement  $\mathbf{V}(\mathbf{R}) = \mathbf{u}(\mathbf{R}) + v_\perp(\mathbf{R})\hat{\mathbf{z}}$ , where  $\mathbf{r}$  and  $\mathbf{u}$  are in-plane and  $\hat{\mathbf{z}}$  is the layer normal. Expanding  $\mathbf{V}(\mathbf{R})$  to second order in  $z$ , imposing symmetry around  $z = 0$  and requiring  $\mathbf{V}(\mathbf{R}) = 0$  at  $z = \pm a/2$  we get an approximate form for the displacement<sup>1</sup>,

$$\mathbf{V}(\mathbf{R}) = (1 - 2z/a)(1 + 2z/a)\mathbf{u}(\mathbf{r}), \quad (1)$$

reminiscent of the quadratic flow profile that underpins the theory of viscous fingering [2]. Soft incompressible solids are well modeled by the neo-Hookean energy density  $\frac{1}{2}\mu(\text{Tr}(F \cdot F^T) - 3)$ , where  $F_{\alpha\beta} = \delta_{\alpha\beta} + \partial_\beta \mathbf{V}_\alpha$ , and incompressibility requires  $\text{Det}(F) = 1$ . Implementing in-

compressibility in a depth-averaged sense we define our 2-d energy density by

$$L = \int_{-a/2}^{a/2} \frac{1}{2}\mu(\text{Tr}(F \cdot F^T) - 3) - P(\text{Det}(F) - 1) dz. \quad (2)$$

The quadratic form for  $\mathbf{V}$  gives  $F = I + (1 - 4z^2/a^2)\nabla\mathbf{u}(\mathbf{r}) - 8z/a^2\mathbf{u}(\mathbf{r})\hat{\mathbf{z}} + \mathbf{z}\mathbf{z}$ , where  $I$  and  $\nabla$  are the in-plane identity and gradient. Conducting the thickness ( $z$ ) integral gives

$$L(\mathbf{u}, P) = \frac{5a}{6} \left( \frac{1}{2}\mu(\text{Tr}(G \cdot G^T) - 2) + \frac{16}{5}\mu \frac{\mathbf{u} \cdot \mathbf{u}}{a^2} - P(\text{Det}(G) - 1) \right) \quad (3)$$

where  $G = I + \frac{4}{5}\nabla\mathbf{u}$  is an effective 2-d deformation gradient, and  $P$  is a 2-d pressure. Minimizing the elastic energy  $E = \int L dA$  over  $\mathbf{u}$  and  $P$  leads to the Euler-Lagrange equations

$$\frac{8\mu}{a^2}\mathbf{u} = \frac{4\mu}{5}\nabla^2\mathbf{u} - \text{Det}(G)G^{-T} \cdot \nabla P \quad (4)$$

$$\text{Det}(G) = 1. \quad (5)$$

To derive the associated boundary conditions, we imagine a small additional displacement  $\delta\mathbf{u}$  that gives rise to a change in  $E$  arising at the boundary  $\delta E = \frac{2a}{3} \oint \delta\mathbf{u} \cdot (\mu G - P \text{Det}(G) G^{-T}) \cdot \hat{\mathbf{n}} ds$ , where  $\hat{\mathbf{n}}$  is the boundary's outward normal. At a free boundary  $\delta E$  would vanish. At an interface with fluid at pressure  $P_f$  we must add the virtual work term  $-P_f V_f$  ( $V_f$  is the fluid volume) to  $E$ , generating an additional boundary term  $-P_f \delta V_f$ . A small patch of boundary at height  $z$ , thickness  $dz$  and in-plane extent  $ds$  has initial vector area  $d\mathbf{A} = dz ds \hat{\mathbf{n}}$ . After deformation, this becomes  $\text{Det}(F) F^{-T} \cdot d\mathbf{A}$ . An incremental displacement  $\delta\mathbf{u}$  displaces the patch by  $(1 - 4z^2/a^2)\delta\mathbf{u}$  and hence changes the fluid volume by  $-(1 - 4z^2/a^2)\delta\mathbf{u} \cdot \text{Det}(F) F^{-T} \cdot d\mathbf{A}$ . Integrating this over the boundary gives  $\delta V_f = -\oint \delta\mathbf{u} \cdot \int_{-a/2}^{a/2} (1 - 4z^2/a^2) \text{Det}(F) F^{-T} dz \cdot \hat{\mathbf{n}} ds$ . Conducting the  $z$  integral then gives  $\delta V_f = -\frac{2a}{3} \oint \delta\mathbf{u} \cdot \text{Det}(G) G^{-T} \cdot \hat{\mathbf{n}} ds$  and hence the appropriate boundary conditions are

$$(\mu G + (P_f - P) \text{Det}(G) G^{-T}) \cdot \hat{\mathbf{n}} = 0, \quad (6)$$

which, with eqns (4-5), specify the problem.

We first solve these equations for fingering in a simple Cartesian geometry to uncover the basic mechanisms at play, considering an elastic layer in an infinite strip with  $0 < y < l$  and  $-\infty < x < \infty$ , an invading fluid at pressure  $P_f$  for  $y < 0$  and a vacuum for  $y > l$ . We expect fingering of the  $y = 0$  boundary at a critical  $P_f$ , so we write the fields as a translationally invariant base-state plus a small perturbation:

$$\mathbf{u} = Y_1(y)\hat{\mathbf{y}} + \epsilon\mathbf{u}_2(\mathbf{x}, y), \quad P = P_1(y) + \epsilon P_2(x, y). \quad (7)$$

Substituting these into eqns (4-5) and setting  $\epsilon = 0$ , we see that  $Y_1$  is a constant and  $P_1$  is linear in  $y$ . Applying eqn. (6) at  $y = 0$  and at  $y = l$  (where  $P_f = 0$ ) then yields:

$$Y_1(y) = a^2 P_f / (8l\mu), \quad P_1(y) = \mu + P_f - P_f y/l. \quad (8)$$

<sup>1</sup>Fig. 1d shows a non-quadratic profile, but the finger is in the non-linear regime well past the point of instability.

Expanding eqns (4-6) to  $\mathcal{O}(\epsilon)$  around this state gives us an eigenvalue problem for the base state's stability:

$$\frac{8\mu}{a^2} \mathbf{u}_2 = \frac{4\mu}{5} \nabla^2 \mathbf{u}_2 - \nabla P_2 + \frac{4}{5} \nabla P_1 \cdot (\nabla \mathbf{u}_2) \quad (9)$$

$$\nabla \cdot \mathbf{u}_2 = 0, \quad (10)$$

$$\left(\frac{4}{5}\mu \nabla \mathbf{u}_2 - P_2 + \frac{4}{5}\mu (\nabla \mathbf{u}_2)^T\right) \cdot \hat{\mathbf{n}} = 0. \quad (11)$$

Assuming explicit oscillatory perturbative fields,  $P_2 = P_2(y) \cos(kx)$ ,  $\mathbf{u}_2 = Y_2(y) \cos(kx) \hat{\mathbf{y}} + X_2(y) \sin(kx) \hat{\mathbf{x}}$ , we solve these equations and see that, provided  $l \gg a$ , the boundary destabilizes when

$$P_f = \frac{2\mu l}{5a} \frac{a^2 k^2 (ak (ak - \sqrt{a^2 k^2 + 10}) + 10) + 25}{ak}. \quad (12)$$

Minimizing this threshold over  $k$ , we see that fluid-driven fingering of a rectilinear elastic meniscus occurs with wavelength and pressure

$$\lambda \approx 2.75...a \quad P_f \approx 10.1...l\mu/a. \quad (13)$$

We next consider the experimental circular geometry [1]. A naive extrapolation of our Cartesian stability analysis result to the circular case by taking  $l \sim r_2 - r_1$  would predict threshold pressures far beyond those observed because the Cartesian base-state is 1-D whereas in the circular one is 2-d, with different qualitative forms for the decay of the elastic fields. Assuming an annular elastic layer occupying the region  $r_1 < r < r_2$ ,  $-\pi < \theta < \pi$  with a fluid at pressure  $P_f$  in the cavity  $r < r_1$  and a vacuum for  $r > r_2$  allows us to write the displacement and pressure fields as

$$\mathbf{u} = R_1(r) \hat{\mathbf{r}} + \epsilon(R_2(r) \cos(n\theta) \hat{\mathbf{r}} + \Theta_2(r) \sin(n\theta) \hat{\boldsymbol{\theta}}) \quad (14)$$

$$P = P_1(r) + \epsilon P_2(r) \cos(n\theta). \quad (15)$$

Substituting these expressions into (4-5), then setting  $\epsilon = 0$ , allows us to solve (5) for  $R_1$ ,

$$R_1(r) = \frac{5r}{4} \left( \sqrt{1 + \left(\frac{c_4}{r}\right)^2} - 1 \right), \quad (16)$$

where the integration constant  $c_4$  parameterizes the inner boundary's displacement. We can solve for  $P_1$  analytically then solve the perturbative equations (9-11) numerically to find the fingering threshold and mode without further approximation (see Appendix) but the algebra is cumbersome. However, the expressions simplify in the limit of thin layers,  $a \ll r_1$ , a case of much interest. As in the Cartesian geometry, we expect an instability when  $R_1(r_1) \sim a$ , when strains become geometrically large. Such displacements require  $c_4 \sim \sqrt{r_1 a} \ll r_1$ , so  $R_1$  can be replaced by its first order expansion  $R_1(r) = 5c_4^2/(8r)$ . Furthermore,  $R_1'(r) \sim c_4^2/r^2$  is negligibly small so we can neglect gradients of  $\mathbf{u}$ , setting  $G = I$ . This reduces eqn. (4) to  $\frac{8\mu}{a^2} R_1(r) = -P_1'(r)$ , which on integration yields

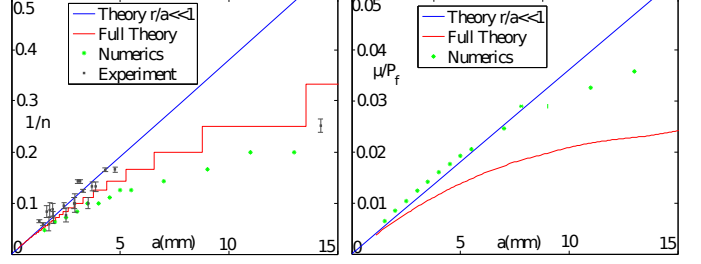


Fig. 2: A thin annular elastic layer with thickness  $a$ , shear modulus  $\mu$  and radius  $r_2 = 125\text{mm}$  has a central cavity of radius  $r_1 = 11.5\text{mm}$  filled with a fluid at pressure  $P_f$ . Above a threshold  $P_f$ , fingers of fluid invades the layer. We show the inverse number of fingers  $1/n$  (left) and the inverse scaled threshold pressure  $\mu/P_f$  (right) as a function of the layer thickness. The plots compare the predictions of the full 2D theory based on eqn. (16) (red lines), the asymptotic results for  $a/r_1 \ll 1$  given in eqn. (19) (blue lines), full finite-element results and, in the left plot, experimental results [1].

$P_1 \sim \log(r)$ . Similarly applying the boundary conditions (6) allows us to determine  $R_1, P_1$  as:

$$R_1(r) = \frac{a^2 P_f}{8\mu r \log(r_2/r_1)}, P_1(r) = \mu + \frac{P_f \log(r/r_2)}{\log(r_1/r_2)}. \quad (17)$$

Both fields only vary on length-scales comparable to  $r_1$ , so around the inner boundary ( $|r - r_1| \ll r_1$ ) they are well described by their Taylor expansions around  $r_1$ :

$$R_1 = \frac{a^2 P_f}{8\mu r_1 \log(r_2/r_1)}, P_1 = \mu + P_f + \frac{P_f(r - r_1)}{r_1 \log(r_1/r_2)}. \quad (18)$$

Identifying  $(r - r_1) \rightarrow y$  and  $r_1 \log(r_2/r_1) \rightarrow l$ , these results match the base state for the rectilinear case (eqn. (8)). Fingering only occurs within a characteristic distance  $a$  from the boundary where base states match, so the instability will proceed in the same way with mode-number ( $n = 2\pi r_1/\lambda$ ) and threshold

$$n \approx 2.28 r_1/a, \quad P_f \approx 10.1 \mu(r_1/a) \log(r_2/r_1). \quad (19)$$

This pressure diverges logarithmically as  $r_2 \rightarrow \infty$  so fingering will occur in a pressurized cavity in an almost infinite layer, but not in a wide rectilinear strip.

In Fig. 2, we compare these predictions with experiments [1] and nonlinear finite element simulations carried out using a commercial package ABAQUS, using a pressure-based Lagrange multiplier method to enforce incompressibility to within  $10^{-9}$  variations in the pressure, and see that that the numerical results agree well with the theory and experiments for very thin layers. Our data extends to layers with  $a/r_1 \gtrsim 1$  which are not thin; unsurprisingly, here the depth-averaged asymptotic theory predicts too few fingers and too high pressures. A better approximation can be obtained by returning to the full expression for  $R_1(r)$  (eqn. (16)) and continuing the derivation without assuming  $a \ll r_1$  (see SI), and are also

shown in Fig. 2. The theory is still depth-averaged so that it cannot capture the full behavior of thick layers, but it captures the qualitative nature of the non-linear deviations.

As alluded to in our introduction, fingering of a confined elastic layer can also be driven by transverse displacement [21, 22]. Layer incompressibility implies that pulling the plates apart causes the meniscus to be inwardly displaced and, at a critical separation, fingers form in a manner reminiscent of Fig. 1. The similarity arises despite the difference in the origin of the base-states because both add volume to an incompressible layer, resulting in long-ranged displacements that only vary on in-plane length-scales. In the boundary region of characteristic width  $a$  where fingering occurs, both base states are essentially constant inward displacements, and finger identically. We now show how our theory makes this connection concrete. If the invading fluid is removed ( $P_f = 0$ ) and instead the rigid plates are separated to  $z = \pm(a + \Delta z)/2$  we must modify  $\mathbf{V}(\mathbf{R})$  to

$$\mathbf{V}(\mathbf{R}) = (1 - 2z/a)(1 + 2z/a)\mathbf{u}(\mathbf{r}) + z\hat{\mathbf{z}}\Delta z/a. \quad (20)$$

Since separation adds volume to the whole layer area, while the inward displacement only does so at the boundary, for thin wide layers, the  $\Delta z$  required for displacement comparable to  $a$  will be small. Assuming  $\Delta z/a \ll 1$ , the above  $\mathbf{V}$  leads to the equations of equilibrium [22]

$$\frac{8\mu}{a^2}\mathbf{u} = \frac{4\mu}{5}\nabla^2\mathbf{u} - \text{Det}(G)G^{-T} \cdot \nabla P, \quad (21)$$

$$\text{Det}(G) = 1 - 6\Delta z/(5a), \quad (22)$$

$$(\mu G - P \text{Det}(G)G^{-T}) \cdot \hat{\mathbf{n}} = 0, \quad (23)$$

identical to the pressure driven case except the change of driving from  $P_f$  in the b.c. to  $6\Delta z/(5a)$  in eqn. (22).

In the Cartesian strip geometry, we can solve eqn. (22) for the translationally invariant displacement  $Y_1(y) = \frac{3}{4}a(l\Delta z/a^2)(1 - 2(y/l))$ , which is symmetric about  $y = l/2$  and hence substantially different from the pressure driven case. However, since this displacement only varies over distances comparable to  $l$ , in a region of width comparable to  $a$  around the  $y = 0$  boundary, it is essentially constant,  $Y_1(0) = \frac{3}{4}l\Delta z/a$ . Substituting this constant into eqns. (21) and (23), we see that, in the same boundary region, the pressure is given by  $P = \mu - 6\mu y\Delta z/a^3$ . Thus, identifying  $\Delta z \rightarrow a^3 P_f/(6l^2\mu)$ , in this boundary region the separation-driven fields match the pressure driven ones (eqn. (8)), up to an offset  $P_f$  in the pressure.

We next consider the stability of these base states by considering small perturbations,  $P = P_1(y) + \epsilon P_2(x, y)$  and  $\mathbf{u} = \mathbf{u}_1(y) + \epsilon \mathbf{u}_2(x, y)$ , localized to the  $y = 0$  boundary. If we expand eqns. (21-23) to first order in  $\epsilon$ , this is analogous to deriving eqns (9-11). The only two differences are the offset in the base pressures by  $P_f$ , which simply cancels the offset by  $P_f$  between the two boundary conditions, and the  $6\Delta z/(5a)$  term in eqn. (22) which, in the thin

layer limit, is negligibly small. Thus the stability of a thin layer is also governed by eqns. (9-11), and the instability proceeds in the same way, with threshold  $\Delta z \approx 1.68a^2/l$ . The same reasoning applies even with large perturbations, so the full non-linear finger development is identical.

In the annular geometry, we solve eqn. (22) for the base state to get  $R_1(r) = \frac{5r}{4} \left( \sqrt{1 - \frac{6\Delta z}{5a} + \left(\frac{c_4}{r}\right)^2} - 1 \right)$ . As in the pressure-driven case, for thin layers with  $a/r_1 \ll 1$ , we may expand the root in the previous expression to get  $R_1(r) = \frac{5c_4^2}{8r} - \frac{3\Delta z r}{4a}$ . Solving eqns (21-23) for the full base state then yields

$$P_1(r) = \mu + \quad (24)$$

$$\frac{3\Delta z \mu}{a^3 \log(r_1/r_2)} \left( r^2 \log\left(\frac{r_1}{r_2}\right) + r_1^2 \log\left(\frac{r_2}{r}\right) + r_2^2 \log\left(\frac{r}{r_1}\right) \right) \\ R_1(r) = \frac{3\Delta z (r_1^2 - r_2^2)}{8ar \log(r_1/r_2)} - \frac{3\Delta z r}{4a}. \quad (25)$$

These fields vary on length-scales comparable to  $r_1 \gg a$ , so in a region around the inner boundary with characteristic width  $a$  they are well approximated by their Taylor series around  $r_1$ . Identifying

$$\Delta z \rightarrow \frac{P_f}{3\mu} \frac{a^3}{2r_1^2 \log(r_1/r_2) - r_1^2 + r_2^2}, \quad (26)$$

we see that the equivalent series differ from those in the pressure driven case (eqn. 18) by the same offset of  $P_f$  to  $P_1$  as in the Cartesian strip case. Thus, as before, the base states differ on long length scales but match around the inner boundary, and are susceptible to exactly the same fingering instability. Substituting the threshold pressure into the above expression for  $\Delta z$ , we find the threshold separation for fingering which, when  $r_2 \gg r_1$ , reduces to  $\frac{\Delta z}{a} \approx 3.37 \frac{a}{r_2} \frac{r_1}{r_2} \log(r_2/r_1)$ , and is indeed small.

We confirm this equivalence between fluid and displacement-driven fingering via nonlinear finite element simulations using the commercial package ABAQUS, with incompressibility implemented using a pressure based penalty method to an accuracy of  $10^{-9}$ . Fig. 3 shows the hysteresis loops and fingering patterns for the two cases. Despite the layers being only modestly thin ( $r_1/a \sim 0.3$ ), the loops are very similar. The fingering transition is sub-critical in both cases, and hence both systems exhibit bistability.

Our study highlights the geometrical similarity and the essential physical differences between elastic and viscous fingering. Elastic fingering is governed by an equilibrium subcritical bifurcation that is reversible whilst viscous fingering is a rate-dependent dynamic process with a supercritical bifurcation driven by a competition between surface tension ( $\gamma$ ) and viscous shear/pressure gradients. Furthermore, we also show that both displacement-controlled and pressure-controlled scenarios may be described by the same theory, contrary to what might be expected. Although we have ignored the effect of surface

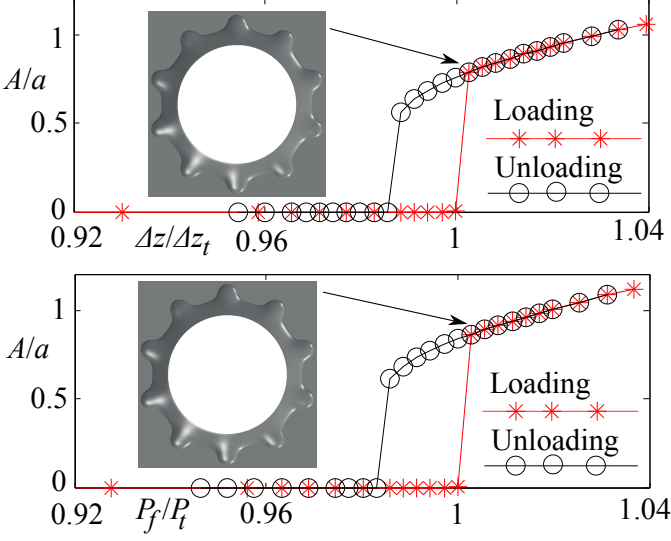


Fig. 3: Finite element hysteresis loops showing finger amplitude  $A$  for displacement (top) and fluid pressure (bottom) driven fingering, using  $a = 3.5\text{mm}$   $r_1 = 11.5\text{mm}$  and  $r_2 = 125\text{mm}$ . Both show a first order transition to very similar fingered states, (see insets) at threshold separation  $\Delta z_t = 0.02a$  and pressure  $P_t = 69.4\mu$  respectively. The dimensionless threshold ratio  $(P_t/\mu)/(\Delta z_t/a) = 3510 \pm 10$  is close to theoretical estimate of 3640 from eqn. (26).

forces, surface tension will become important in elastic fingering if the layer thickness becomes comparable to the elastocapillary length scale  $\gamma/\mu$ . These may be relevant to many phenomena in adhesion science/engineering and perhaps even biological morphogenetic processes where branching and fingering abound.

\*\*\*

We thank E. Bouchaud and B. Saintyves for introducing us to this experiment, for useful discussions and Fig. 1c,d. We also thank Trinity Hall, Cambridge and the 1851 Royal Commission (JSB), the Harvard NSF-MRSEC DMR0820484 (ZW,LM) and the MacArthur Foundation (LM) for partial support.

## REFERENCES

- [1] SAINTYVES B., DAUCHOT O. and BOUCHAUD E., *Phys. Rev. Lett.*, **111** (2013) 047801.
- [2] SAFFMAN P. and TAYLOR G., *Proc. R. Soc. Lond. A.*, **245** (1958) 312.
- [3] BATAILLE J., *Revue Inst. Pétrole*, **23** (1968) 1349.
- [4] NITTMAN J., DACCORD G. and STANLEY M., *Nature*, **314** (1985) 391.
- [5] PARK S. and DURIAN D., *Phys. Rev. Lett.*, **72** (1994) 3347.
- [6] AMAR M. B. and POIRÉ E. C., *Phys. Fluids*, **11** (1999) 1757.
- [7] LINDNER A., BONN D., POIRÉ E. C., AMAR M. B. and MEUNIER J., *J. Fluid Mech.*, **469** (2002) 237.

- [8] KONDIC L., SHELLEY M. J. and PALFFY-MUHORAY P., *Phys. Rev. Lett.*, **80** (1998) 1433.
- [9] KAWAGUCHI M., *Nonlin. Anal.: Theory, Meth. & App.*, **47** (2001) 907.
- [10] COUSSOT P., *J. Fluid Mech.*, **380** (1999) 363.
- [11] LINDNER A., COUSSOT P. and BONN D., *Phys. Rev. Lett.*, **85** (2000) 314.
- [12] MORA S. and MANNA M., *Phys. Rev. E*, **80** (2009) 016308.
- [13] HIRATA T., *Phys. Rev. E*, **57** (1998) 1772.
- [14] LEMAIRE E., LEVITZ P., DACCORD G. and VAN DAMME H., *Phys. Rev. Lett.*, **67** (1991) 2009.
- [15] WILSON S., *J. Fluid Mech.*, **220** (1990) 413.
- [16] MORA S. and MANNA M., *J. Non-Newt. Fluid Mech.*, **173** (2012) 30.
- [17] MORA S. and MANNA M., *Phys. Rev. E*, **81** (2010) 026305.
- [18] NASE J., LINDNER A. and CRETON C., *Phys. Rev. Lett.*, **101** (2008) 074503.
- [19] GHATAK A., CHAUDHURY M., SHENOY V. and SHARMA A., *Phys. Rev. Lett.*, **85** (2000) 4329.
- [20] ADDA-BEDIA M. and MAHADEVAN L., *Proc. Roy. Soc. Lond. A*, **462** (2006) 3233.
- [21] SHULL K., FLANIGAN C. and CROSBY A., *Phys. Rev. Lett.*, **84** (2000) 3057.
- [22] BIGGINS J. S., SAINTYVES B., WEI Z., BOUCHAUD E. and MAHADEVAN L., *Proc. Nat. Acad. Sci. USA*, **110** (2013) 12545.

**APPENDIX.** — Here, we provide the details of the calculation for the fingering threshold and mode in an annular layer, continuing from eqn 16. In an  $(r, \theta)$  circular polar coordinate system we note that,

$$\nabla P = \begin{pmatrix} P_{,r} \\ P_{,\theta} \\ r \end{pmatrix} \quad \nabla \mathbf{u} = \begin{pmatrix} u_{r,r} & \frac{u_{r,\theta} - u_{\theta}}{r} \\ u_{\theta,r} & \frac{u_{\theta,\theta} + u_r}{r} \end{pmatrix} \quad (\text{A.1})$$

$$\nabla^2 \mathbf{u} = \begin{pmatrix} u_{r,rr} + \frac{u_{r,\theta\theta}}{r^2} + \frac{u_{r,r}}{r} - \frac{2u_{\theta,\theta}}{r^2} - \frac{u_r}{r^2} \\ u_{\theta,rr} + \frac{u_{\theta,\theta\theta}}{r^2} + \frac{u_{\theta,r}}{r} + \frac{2u_{r,\theta}}{r^2} - \frac{u_{\theta}}{r^2} \end{pmatrix}. \quad (\text{A.2})$$

where  $A_{,b} = \partial A / \partial b$ . We find the base pressure,  $P_1(r)$ , by considering the  $\hat{\mathbf{r}}$  component of eqn. 4 which, for a radial base state displacement  $R_1(r)\hat{\mathbf{r}}$ , reduces to

$$\frac{8\mu}{a^2} R_1(r) = \frac{4\mu}{5} \left( \frac{rR_1'(r) - R_1(r)}{r^2} + R_1(r) \right) + \left( 1 + \frac{4R_1(r)}{5r} \right) P_1'(r). \quad (\text{A.3})$$

Substituting in  $R_1$  from eqn. (16) and simplifying gives

$$a^2 r (c_4^2 + r^2)^2 P_1'(r) + \mu \left( a^2 c_4^4 + 10r^2 (c_4^2 + r^2) \left( -r\sqrt{c_4^2 + r^2} + c_4^2 + r^2 \right) \right) = 0 \quad (\text{A.4})$$

which we can solve to find  $P_1(r)$  as

$$P_1 = P_0 - \mu \left( \frac{5r^2}{a^2} \left( 1 - \sqrt{\frac{c_4^2}{r^2} + 1} \right) + \frac{c_4^2}{2(c_4^2 + r^2)} + \frac{5c_4^2}{a^2} \log \left( \sqrt{c_4^2 + r^2} + r \right) - \log \left( \sqrt{\left( \frac{c_4}{r} \right)^2 + 1} \right) \right), \quad (\text{A.5})$$

where  $P_0$  is a constant of integration. Applying the boundary condition, eqn. 6, on the inner and outer radii, gives

$$\mu \left( 1 + \frac{4}{5} R_1'(r_1) \right) + (P_f - P_1(r_1)) \left( 1 + \frac{4R_1(r_1)}{5r_1} \right) = 0 \quad (\text{A.6})$$

$$\mu \left( 1 + \frac{4}{5} R_1'(r_2) \right) - P_1(r_2) \left( 1 + \frac{4R_1(r_2)}{5r_2} \right) = 0. \quad (\text{A.7})$$

For algebraic convenience, instead of solving these for the integration constant,  $P_0$  and  $c_4$ , in terms of the applied pressure  $P_f$ , we solve them for  $P_f$  and  $P_0$  in terms of  $c_4$ :

$$\begin{aligned} \frac{P_0}{\mu} = & \frac{5r_2^2}{a^2} \left( 1 - \sqrt{\frac{c_4^2}{r_2^2} + 1} \right) + \frac{5c_4^2}{a^2} \log \left( \sqrt{c_4^2 + r_2^2} + r_2 \right) \\ & - \frac{c_4^2}{2(c_4^2 + r_2^2)} - \frac{1}{2} \log \left( \frac{c_4^2}{r_2^2} + 1 \right) + 1 \end{aligned} \quad (\text{A.8})$$

$$\begin{aligned} \frac{2P_f}{\mu} = & \frac{10c_4^2}{a^2} \log \left( \frac{\sqrt{c_4^2 + r_2^2} + r_2}{\sqrt{c_4^2 + r_1^2} + r_1} \right) + \\ & 10 \left( \frac{r_1^2}{a^2} \left( \sqrt{1 + \left( \frac{c_4}{r_1} \right)^2} - 1 \right) - \frac{r_2^2}{a^2} \left( \sqrt{1 + \left( \frac{c_4}{r_2} \right)^2} - 1 \right) \right) \\ & - \frac{r_1^2}{c_4^2 + r_1^2} + \log \left( \frac{c_4^2}{r_1^2} + 1 \right) + \frac{r_2^2}{c_4^2 + r_2^2} - \log \left( \frac{c_4^2}{r_2^2} + 1 \right). \end{aligned} \quad (\text{A.9})$$

This fully specifies the base state. If we have a generic base state  $\mathbf{u}_1$  and  $P_1$  giving rise to an effective deformation gradient  $G_1$ , and we add small perturbations

$$\mathbf{u} = \mathbf{u}_1 + \epsilon \mathbf{u}_2 \quad P = P_1 + \epsilon P_2 \quad (\text{A.10})$$

then expanding eqns. (4-6) about the base state to first order in  $\epsilon$  yields

$$\frac{8\mu}{a^2} \mathbf{u}_2 = \frac{4\mu}{5} \nabla^2 \mathbf{u}_2 - \nabla P_2 \cdot \text{adj}(G_1) - \frac{4}{5} \nabla P_1 \cdot \text{adj}(\nabla \mathbf{u}_2) \quad (\text{A.11})$$

$$\text{Tr}(\text{adj}(G_1) \cdot \nabla \mathbf{u}_2) = 0 \quad (\text{A.12})$$

subject to the boundary conditions

$$\begin{aligned} & \left( \mu \frac{4}{5} \nabla \mathbf{u}_2 - P_2 \text{adj}(G_1)^T \right. \\ & \quad \left. + \frac{4}{5} (P_f - P_1) \text{adj}(\nabla \mathbf{u}_2)^T \right) \cdot \hat{\mathbf{n}} = 0, \end{aligned} \quad (\text{A.13})$$

where  $\text{adj}$  denotes the adjugate matrix.

Linearizing about the circular base-state, we assume oscillatory forms for the perturbations

$$\mathbf{u} = R_1(r) \hat{\mathbf{r}} + \epsilon (R_2(r) \cos(n\theta) \hat{\mathbf{r}} + \Theta_2(r) \sin(n\theta) \hat{\boldsymbol{\theta}}) \quad (\text{A.14})$$

$$P = P_1(r) + \epsilon P_2(r) \cos(n\theta), \quad (\text{A.15})$$

from which we get

$$\nabla \mathbf{u}_2 = \begin{pmatrix} R_2'(r) \cos(n\theta) & -\frac{nR_2(r) + \Theta_2(r)}{r} \sin(n\theta) \\ \Theta_2'(r) \sin(n\theta) & \frac{R_2(r) + n\Theta_2(r)}{r} \cos(n\theta) \end{pmatrix} \quad (\text{A.16})$$

$$\nabla P_2 = \begin{pmatrix} P_2'(r) \cos(n\theta) \\ -nP_2(r) \sin(n\theta) \end{pmatrix} \quad (\text{A.17})$$

so, the  $\theta$  component of eqn. (A.11) is an algebraic equation for  $P_2(r)$  with the solution

$$\begin{aligned} P_2(r) = & \frac{4(\Theta_2(r)(\mu(a^2(n^2 + 1) + 10r^2) + a^2rP_1'(r)))}{a^2nr(4R_1'(r) + 5)} \\ & + \frac{4(a^2nR_2(r)(2\mu + rP_1'(r)) - a^2\mu r(r\Theta_2''(r) + \Theta_2'(r)))}{a^2nr(4R_1'(r) + 5)} \end{aligned} \quad (\text{A.18})$$

and similarly, since  $G_1$  is diagonal, eqn. (A.12) is an algebraic equation for  $\Theta_2$  with the solution

$$\begin{aligned} \Theta_2(r) = & -\frac{(4R_1(r) + 5r)R_2'(r)}{n(4R_1'(r) + 5)} - \frac{R_2(r)}{n} \\ = & -\frac{(c_4^2 + r^2)R_2'(r) + rR_2(r)}{nr}. \end{aligned} \quad (\text{A.19})$$

The  $r$  component of eqn (A.11) yields an ode for  $R_2(r)$ :

$$\begin{aligned} & a^2(4R_2(r)(\mu + \mu n^2 + rP_1'(r)) + 4n\Theta_2(r)(2\mu + rP_1'(r)) \\ & + r((4R_1(r) + 5r)P_2'(r) - 4\mu(rR_2''(r) + R_2'(r)))) \\ & + 40\mu r^2 R_2(r) = 0. \end{aligned} \quad (\text{A.20})$$

Substituting in the above forms for  $R_1$ ,  $P_1$ ,  $\Theta_2$  and  $P_2$  yields a non-linear fourth order differential equation. It is accompanied by the four boundary conditions given by applying eqn. A.13 on the inner and outer radii:

$$4(P_f - P_1(r_1))(n\Theta_2(r_1) + R_2(r_1)) \quad (\text{A.21})$$

$$- P_2(r_1)(4R_1(r_1) + 5r_1) + 4\mu r_1 R_2'(r_1) = 0$$

$$(P_f - P_1(r_1))(nR_2(r_1) + \Theta_2(r_1)) + \mu r_1 \Theta_2'(r_1) = 0 \quad (\text{A.22})$$

$$4P_1(r_2)(n\Theta_2(r_2) + R_2(r_2)) \quad (\text{A.23})$$

$$+ P_2(r_2)(4R_1(r_2) + 5r_2) - 4\mu r_2 R_2'(r_2) = 0$$

$$P_1(r_2)(nR_2(r_2) + \Theta_2(r_2)) - \mu r_2 \Theta_2'(r_2) = 0. \quad (\text{A.24})$$

We solve the system (A.20-A.24) using the Matlab's `bvp4c` boundary value solver by specifying values for  $n$ ,  $r_1$ ,  $r_2$  and  $a$  to find the lowest value of  $c_4$  for which the equations have a solution, and find the solution. We then iterate over  $n$  until we find the solution with the lowest value of  $c_4$  (that is the lowest displacement on the inner boundary), to find the first unstable mode, which sets the threshold and mode-number for fingering. We finally use eqn. (A.9) to recover the fluid pressure threshold from the value of  $c_4$ . The threshold and mode-number predictions from this procedure are shown in Fig. 2 in our main text.